An unprecedented non-classical polyinterhalogen anion made of $[I_2Cl]^-$ and I_2 at the 2-(*p*-tolyl)selenopheno[2,3-*b*]pyridinium cation template†

M. Carla Aragoni,[a] Enrico Podda,[ab] Massimiliano Arca,[a] Anna Pintus,*[a] Vito Lippolis,*[a] Claudia Caltagirone,[a] Ricardo H. Bartz,[c] Eder J. Lenardão,[c] Gelson Perin,[d] Ricardo F. Schumacher,[d] Simon J. Coles[e] and James B. Orton[e]

The reactivity between 2-(*p*-tolyl)selenopheno[2,3-*b*]pyridine (**L**) and ICl in MeCN is presented. Single crystal structure analysis revealed the formation of two distinct crystalline materials both featuring the protonated 2-(*p*-tolyl)selenopheno[2,3-*b*]pyridinium cation $[H\mathbf{L}]^+$. Colourless crystals were identified as the dihydrate salt $[H\mathbf{L}]Cl{\cdot}2H_2O$ (**1**), and dark-red crystals as compound $\{[H\mathbf{L}]^+[I_2Cl]^-\}_3{\cdot}1/2I_2$ (**2**) that features the peculiar presence of the rare non-classical $[I_2Cl]^-$ interhalide. Halogen Bonds (XBs) between the cocrystallized I_2 molecule and $[I_2Cl]^-$ anions led to the novel overall discrete $[I_{10}Cl_4]^{4-}$ *H*-shaped polyinterhalide formation, which is stabilized through hydrogen bonds (HBs) with the templating $[H\mathbf{L}]^+$ cations. The experimental observations are supported by extensive theoretical calculations at the DFT level that were employed to study the role played by non-covalent interactions in the formation of the presented unique polyinterhalide.

Introduction

Non-covalent interactions play a key role in the design and the controlled construction of novel solid-state architectures with implications in many prominent research fields such as supramolecular chemistry, crystal engineering and material chemistry. Among others, the cooperativity and competitivity between directional intermolecular hydrogen bonds (HBs) and halogen bonds (XBs) have been in the spotlight for many decades in view of establishing a hierarchy of interactions between multifunctional synthons with the aim of predicting and exerting synthetic control over both the crystal structure growth/self-assembly processes and the properties of the resulting crystalline solids and commodity chemicals and materials.[1–9]

In this context, polyhalides of the type $[X_n(X_2)_m]^{n-}$ or $[X_{2m+n}]^{n-}$ ($n, m > 0$; X = halogen), and in particular polyiodides (X = I), despite having been studied for at least two centuries, still represent a fascinating class of compounds due to their extremely variegated, unpredictable and puzzling structural chemistry.[10,11] Moreover, their interesting applicative possibilities in photovoltaics,[12,13] halogenation reactions,[14] noble metal recovery[15] as solid-state conductors,[15a,16] and ionic liquids[15a,17] make them particularly appealing.

It is well-established that the tendency of di-halogens and halide ions to catenate and form polyhalides increases on passing from fluorine to iodine. Indeed, a large number of discrete polyiodides[10] and polybromides,[15a] up to $[I_{29}]^{3-}$ and $[Br_{24}]^{2-}$, respectively, have been structurally characterized, and some examples of infinite networks are also known.[10a,11,18] Much less numerous are polychlorides and polyfluorides, and some of them have been observed only spectroscopically under cryogenic conditions in noble-gas matrices.[15a] Recently, polyinterhalides of the type $[X_n(Y_2)_m]^{n-}$ or $[X_n(YZ)_m]^{n-}$ (X, Y, Z = halogen) are also receiving increasing interest because of the potential increased and intriguing structural diversity that they can offer with respect to homonuclear variants.[15a] Generally, polyhalides can be broken down into two components *i.e.*, the Lewis base halides X^- $[X_3^-]$, and the Lewis acid acceptor molecules X_2,

[a] *Dipartimento di Scienze Chimiche e Geologiche, Università degli Studi di Cagliari, S.S. 554 Bivio per Sestu, 09042 Monserrato, CA, Italy. E-mail: lippolis@unica.it, apintus@unica.it*
[b] *Centro Servizi di Ateneo per la Ricerca (CeSAR), Università degli Studi di Cagliari, Cittadella Universitaria – Blocco A, 09042 Monserrato, CA, 09042, Italy*
[c] *Laboratório de Síntese Orgânica Limpa – LASOL, CCQFA, Universidade Federal de Pelotas-UFPel-P.O. Box 354-96010-900, Pelotas, RS, Brazil*
[d] *Departamento de Química, Universidade Federal de Santa Maria, UFSM, 97105-900, Santa Maria, RS, Brazil*
[e] *National Crystallography Service, School of Chemistry, University of Southampton, Southampton, SO17 1BJ, UK*

† Electronic supplementary information (ESI) available. CCDC 2204970 and 2204971. For ESI and crystallographic data in CIF or other electronic format see DOI: https://doi.org/10.1039/d2nj04689j

following halogen-bond formation and supramolecular assembly *via* a charge-transfer interaction involving the HOMO of the former donors and the LUMO (σ*) of the latter acceptors[15a,19] (in the case of X = I, I···I contacts can range from about 2.9 to about 3.6 Å for the formation/definition of discrete polyiodide entities, and from 3.6 up to the sum of the van der Waals radii for the generation of very intricate infinite tri-dimensional networks).[10,11] The nature (size, shape and charge) of the accompanying/templating cation is crucial in determining the extent and the structural and geometrical features of the supramolecular polyanionic species, also due to the ability of halogens to participate both in HBs and XBs in systems featuring the moieties E–H–X and E–X–Y (E = C, N, P, O, S, Se; X, Y = halogen).[10,11,15,18] The simplest strategy to form polyhalide architectures considers the reaction of preformed cations with halide counter-anions in the presence of different amounts of di-halogens. However, in most cases it is possible/convenient to start from neutral Lewis bases and molecular di-halogens or inter-halogens acceptors in different molar ratios and solvents, exploiting the templating cations formed *in situ* by either oxidation or protonation reactions of the donors by the solvent or moisture present in the reaction environment under ambient conditions.

In this context, polypyridyl Lewis bases **B**, differing in the nature and number of nitrogen donor sites, in their dimensions, rigidity, hindrance, and directionality of bonding, represent ideal substrates being capable either to undergo *N*-protonation, thus originating cations $[H_nB]^{n+}$ (n = 1 to k; k = number of pyridyl units in **B**) counterbalancing discrete or extended polyhalide species,[18a,20] or to form CT adducts **B**·nX$_2$.[20a–22] *N*-Halopyridinium ions $[BX]^+$,[23] $[B–X–B]^+$ complexes with two nitrogen donors coordinating a central halide(I),[24] and di-halogen molecules bridging two donor units **B**–X–X–**B**,[22a,25] have also been described, analogous to those reported for the reaction of chalcogen containing molecules with di-halogens and interhalogens.[26] Protonated polypyridyl cations were also found under anhydrous conditions, and even if the protonation mechanism was not extensively investigated,[27] the oxidation of the aromatic heterocycle to give cationic radical species $[B^{\bullet}]^+$ was proposed to be responsible for the formation of stable cationic protonated species by solvolysis or reaction with incipient moisture.[27]

Recently, we have focused our attention on donor molecules featuring the simultaneous presence of both N-heterocyclic and chalcogen Lewis donor sites,[18a,20a,22c,25,28] which should enlarge, at least in principle, both the number of products accessible by reaction with di-halogen or interhalogen acceptors and the structural diversity in the resulting self-assembled polyhalide and polyinterhalides architectures. Among the possible donors featuring these structural features, chalcogenophene-fused pyridines represent an interesting class of compounds extensively exploited in medicinal chemistry as promising drugs for the treatment of autoimmune diseases, in materials science as organic semiconductors, and in organic synthesis.[29] Here we report the results achieved by reacting 2-(*p*-tolyl)selenopheno[2,3-*b*]pyridine (**L**)[29] (Scheme 1) with the inter-halogen acceptor ICl, aiming to assemble unusual polyinterhalides in the solid state.

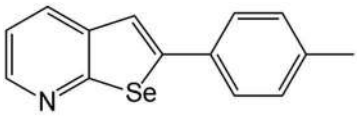

L

Scheme 1 2-(*p*-Tolyl)selenopheno[2,3-*b*]pyridine (**L**).

Results and discussion

Synthesis and characterization

Depending on the chemical environment of the more electronegative halogen, polyinterhalogens of the type $[X_n(Y_2)_m]^{n-}$ or $[X_n(YZ)_m]^{n-}$ (X, Y, Z = halogen) can be described as "classical" and "non-classical": the first class of polyanions features a central electropositive halogen surrounded by more electronegative halogen atoms (*i.e.* $[ICl_2]^-$ and $[ICl_4]^-$); the second is characterized by a more electronegative X^- halide coordinating di-halogen (X_2) or interhalogen (XY) molecules (*i.e.* $[I_2Cl]^-$ and $[Cl(I_2)_4]^-$, limiting examples to Cl^-/I_2 systems).[15] Since interhalogens such as ICl tend to disproportionate in solution, thus allowing for the formation of products, including polyhalides and possibly polyinterhalides, different from the 1 : 1 CT adducts expected upon direct reaction with Lewis bases,[18a,20,22c,30,31] we decided to explore the direct reaction of **L** with ICl under ambient conditions (normally used in a first synthetic approach for reactions of chalcogen containing molecules with di-halogens and interhalogens),[26] in place of the synthetic route commonly used for the preparation of polyhalides and polyinterhalides, which exploits the reaction of dihalides with halide salts. The reaction of **L** with an equimolar amount of ICl in MeCN led to the formation of two distinct crystalline products upon slow evaporation of the solvent at room temperature in air: lath-shaped colourless crystals and dark-red block-shaped crystals. A single crystal X-ray diffraction (XRD) analysis of the former revealed the formation of the dihydrate hydrochloride salt of the ligand [H**L**]Cl·2H$_2$O (**1**) (see Fig. 1 and Table S1 in the ESI†). *N*-Protonation of **L** generated the planar cationic species $[HL]^+$, which is strongly H-bonded to a chloride anion [$d_{D–A}$ (N–H···Cl) = 3.022(2) Å, $\alpha_{N–H–Cl}$ = 174(3)°; see Table S4 in the ESI†]. Moreover, two crystallographically independent clathrate water molecules are observed in the asymmetric unit of **1**. As expected, the water molecules are engaged in hydrogen bonds with the chloride anion.

N–H···Cl and C–H···Cl [$d_{D–A}$ (C–H···Cl) = 3.484(2) Å, $\alpha_{C–H–Cl}$ = 159.2(2)°; see Table S4 in the ESI†] H-bonds enable the formation of dimeric assemblies of two $[HL]^+$ cations bridged by two Cl^- anions (Fig. S1, ESI†). Head-to-tail π–π stacking interactions between these dimeric assemblies determine a layered crystal packing (Fig. S1 and S2, ESI†). A X-ray diffraction analysis on the dark-red block-shaped crystals revealed the structural formulation $\{[HL]^+[I_2Cl]^-\}_3$·1/2I$_2$ (**2**) for the corresponding compound, in agreement with microanalytical data.

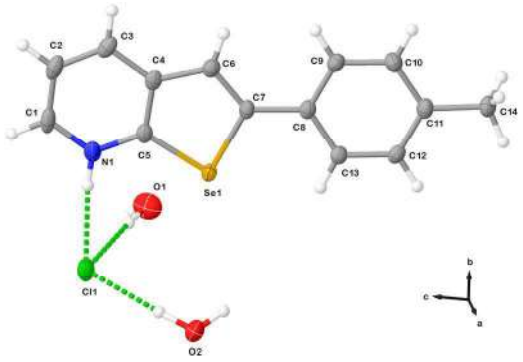

Fig. 1 Crystal structure of the compound [HL]Cl·2H_2O (**1**) with the atom numbering scheme adopted. Displacement ellipsoids are drawn at 50% probability level [for selected bond lengths (Å) and angles (°) see Tables S2–S4 in the ESI†].

The ionic compound crystallizes in the triclinic space group $P\bar{1}$ (see Table S1, ESI†) with three crystallographically independent $[HL]^+$ cations balanced by three independent non-classical $[I_2Cl]^-$ anions and half an I_2 molecule that lies close to an inversion centre (Fig. 2). Each planar $[HL]^+$ cation is H-bonded to an $[I_2Cl]^-$ anion *via* the Cl atom with the trihalide being located almost perpendicular to the plane containing the cation (Fig. 2). The geometrical features of the $[HL]^+$ cations in both crystal structures of compounds **1** and **2** are almost identical (see Tables S2 and S3, ESI†). On passing from **1** to **2**, a slight elongation of the nitrogen to chlorine distance is observed ranging from 3.054(3) to 3.076(3) Å in **2**, which is accompanied by a small deviation from linearity [α_{N-H-Cl} = 153.30(3)–154.62(18)°] resulting from the XB formation between Cl^- and I_2 within the non-classical $[I_2Cl]^-$ interhalides (Table S4, ESI†). Cl–I distances in the Cl–I–I three-body systems range from 2.6947(10) to 2.7779(9) Å (Table S4, ESI†), which are 25–28% shorter than the sum of the relevant van der Waals radii ($\sum R_{vdW\ Cl-I}$ = 3.73 Å),[32] in agreement to that found in other $[I_2Cl]^-$ trihalides.[33,34] The terminal iodine atoms in the $[I_2Cl]^-$ trihalides resulted affected by positional disorder, which was modelled in all cases with a partial occupancy model over two sites (see Experimental section for relevant atomic occupancies and details).

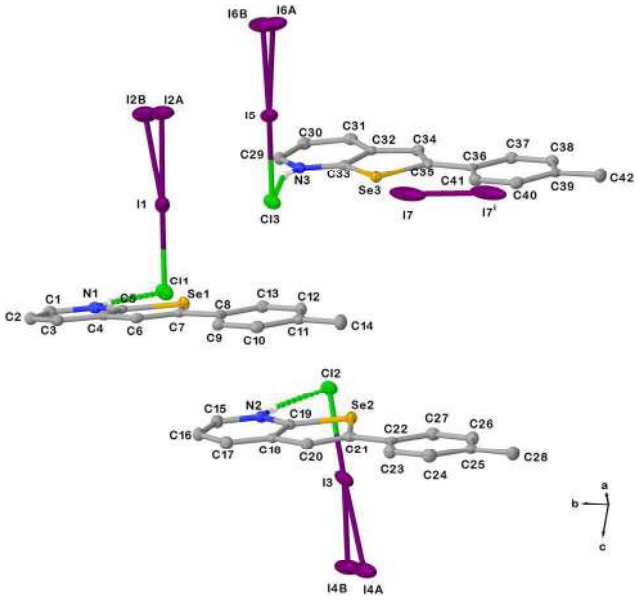

Fig. 2 Crystal structure of compound {$[HL]^+[I_2Cl]^-$}$_3$·1/2I_2 (**2**) with the atom numbering scheme adopted. Only H atoms involved in hydrogen bonds are shown for clarity. Displacement ellipsoids are drawn at 50% probability level [for selected bond lengths (Å) and angles (°) see Tables S2–S4 in the ESI†]. Symmetry code: ^{i} = −*x*, −*y*, −*z*.

The intramolecular I–I distances in the trihalides range from 2.7097(15) to 2.830(6) Å (Table S4, ESI†), which are slightly longer than those found in pure di-iodine in the solid state [2.715(6) Å],[35a] as a consequence of the CT from Cl^- to I_2 in the $[I_2Cl]^-$ anions formation. A similar slight elongation is observed for the co-crystallized I_2 molecule [I7–I7^i = 2.7420(11) Å, see Fig. 2]. Genuine structurally characterized $[I_2Cl]^-$ trihalides are rather rare in the literature.[33,34,36] The $[I_2Cl]^-$ trihalide was structurally characterized in an organic derivative for the first time in the compound {$[phenH]_2^+[I_2Cl]^-[ICl_2]^-$} (phen = 1,10-phenanthroline), obtained from the reaction of phen with a KI/I_2/HCl mixture in methanol.[33] In this compound, $([I_2Cl]^-)_\infty$ infinite chains, H-bonded to $[phenH]^+$ cations, are formed *via* head to tail ···[I–I–Cl]$^-$···[I–I–Cl]$^-$··· interactions of $[I_2Cl]^-$ units [I–I = 2.7371(4), I–Cl = 3.0404(9) and 3.1584(9) Å]. The I–Cl distances within the $[I_2Cl]^-$ units in {$[phenH]_2^+[I_2Cl]^-[ICl_2]^-$} are rather longer than those observed in **2** in agreement with a strong XB between I_2 and Cl^- in the formation of $[I_2Cl]^-$ for the latter. In the crystal packing of **2**, two symmetry-related {$[HL]^+[I_2Cl]^-$} ionic couples are bridged by the co-crystallized di-iodine molecule *via* I···I interactions of 3.289(12) and 3.585(11) Å at the terminal disordered iodine atom of the $[I_2Cl]^-$ units (I6A^{iii}–I7, I6B^{iii}–I7, respectively, Fig. 3) to give *Z*-shaped non-classical $[I_6Cl_2]^{2-}$ assemblies. These, in turn interact at their corners (I6A in Fig. 3) with two other symmetry-related {$[HL]^+[I_2Cl]^-$} ionic couples *via* longer I···I contacts [I6A^{iii}···I2A^{vi} 3.641(6), I6B^{iii}···I2B^{vi} 3.685(8) Å, see Fig. 3] to give overall discrete $[I_{10}Cl_4]^{4-}$ *H*-shaped polyinterhalides anchored by N–H···Cl H-bonds to four $[HL]^+$ cations. The twisted *H*-shaped configuration in the $[I_{10}Cl_4]^{4-}$ polyinterhalide resembles that observed for the $[I_{12}]^{2-}$ polyhalide in $[Ag_2([15]aneS_5)_2]I_{12}$, which was described as a central $[I_4]^{2-}$ interacting at each of its termini with two di-iodine molecules.[37] Non-classical polyinterhalides of I_2 and Cl^- structurally more complex than $[I_2Cl]^-$ are extremely rare in the literature.[15,38] The example described herein, to the best of our knowledge, would be the first in which the chloride atom retains its mono-coordination to one I_2 molecule in an overall *H*-shaped $[I_2Cl^-]_4I_2$ assembly, due to the H-bonds formed with $[HL]^+$ cations at the Cl ends. It is worth noting that one independent {$[HL]^+[I_2Cl]^-$} ionic couple (the one featuring the I4–I3–Cl2 trihalide, Fig. 3) is not involved in the assembly of the *H*-shaped polyinterhalide motif, all distances with neighboring atoms being longer than the sum of the relevant van der Waals radii. The crystal packing of **2** features alternate layers of anionic $[I_{10}Cl_4]^{4-}$ and $[I_2Cl]^-$ moieties and pillared H-bonded $[HL]^+$ cations, which run parallel to the *b*-axis as shown in Fig. 4.

The layers of $[HL]^+$ cations are stabilized by means of intermolecular π–π interactions between parallel pyridyl and *p*-tolyl moieties of slightly slipped adjacent cationic molecules

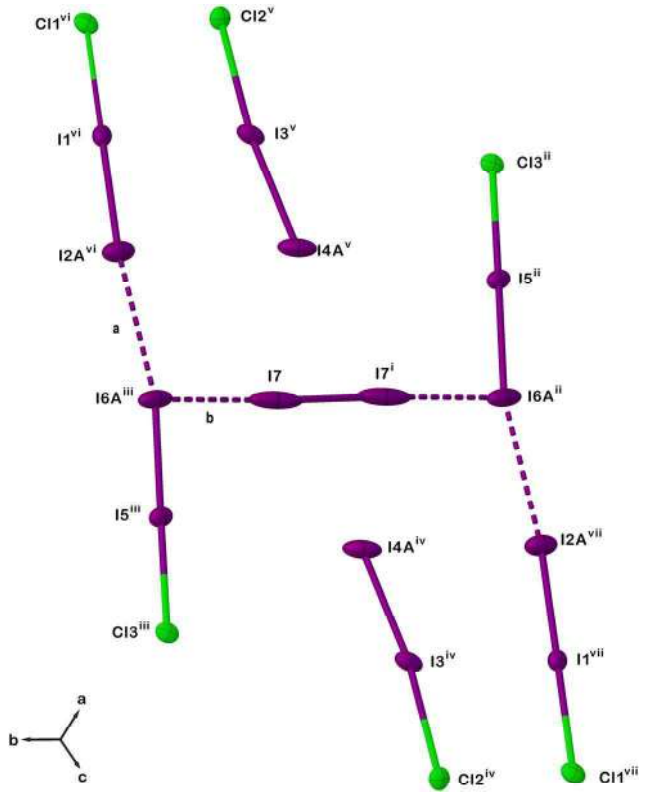

Fig. 3 View along the [111] direction of the unique *H*-shaped polyinterhalide $[I_{10}Cl_4]^{4-}$ assembly in compound **2**. I···I interactions are depicted as **a** and **b** [**a**: I6A^{iii}···I2A^{vi} 3.641(6), I6B^{iii}···I2B^{vi} 3.685(8) Å; **b**: I6A^{iii} ···I7 3.289(12), I6B^{iii}···I7 : 3.585(11) Å]. Disordered minor components (I2B, I4B and I6B) of $[I_2Cl]^-$ anions, and $[HL]^+$ cations are not shown for clarity reasons. Symmetry codes: $^{i} = -x, -y, -z$. $^{ii} = 1 - x, -y, -z$; $^{iii} = -1 + x, +y, +z$; $^{iv} = -x, -y, 1 - z$; $^{v} = +x, +y, -1 + z$; $^{vi} = 1 - x, 1 - y, -z$; $^{vii} = -1 + x, -1 + y, +z$.

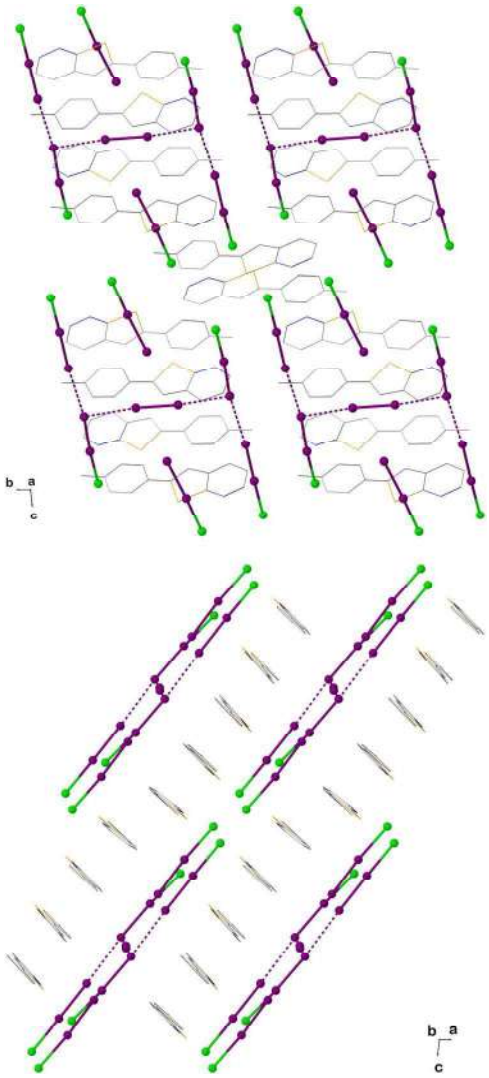

Fig. 4 Packing diagrams of compound **2** along *a* (top) and *b* (bottom) axis, respectively. For clarity, halogen atoms are represented in balls and sticks, $[HL]^+$ cations in wireframe and H atoms are omitted.

(centroid to centroid distances ranging from 3.46–3.60 Å; see Fig. S3 in the ESI†). The description of the polyinterhalide assembly in **2** as $[I_2Cl^-]_4I_2$, agrees with the Raman spectrum of the compound in the low frequency region (see below), which features three main peaks at 171, 157, and 76 cm^{-1} (Fig. S4, ESI†).

Theoretical calculations

Density Functional Theory (DFT) calculations[39] were carried out to gain a deeper insight into the role played by the non-covalent interactions in the formation of **2** and to aid in the interpretation of experimental data. Following previous studies on related systems,[22c] Adamo and Barone's mPW1PEW hybrid functional[40] was adopted along with the LanL2DZ(d,p) basis set (featuring both diffuse and polarization functions)[41] with effective core potentials (ECP).[42,43] The different synthons of **2** were initially studied. The donor ligand was optimized both in its neutral **L** and protonated cationic form $[HL]^+$ starting from structural data (see Table S5–S7, and Fig. S5 in the ESI†). The most stable conformation was calculated to be slightly twisted in both **L** and $[HL]^+$, with a torsion angle τ (Se1–C7–C8–C13 dihedral angle in Fig. 1 and 2 and Fig. S5, ESI†) of about 28 and 24°, respectively. A scan of the potential energy surface (PES) was performed on **L** and $[HL]^+$ at different frozen angles of the *p*-tolyl ring (Fig. S6, ESI†), showing a negligible rotational barrier (lower than 3 kcal mol^{-1}). The almost completely planar conformation observed for $[HL]^+$ in **2** (τ = 0.85–3.93°) can thus be ascribed to the crystal packing, and in particular, the π–π stacking interactions observed between neighboring $[HL]^+$ cations (Fig. 4 and Fig. S3, ESI†). A very good agreement was found between the optimized parameters of $[HL]^+$ and the corresponding average values in **2**, bond distance and angles differing by less than 0.02 Å and 2°, respectively (Table S7, ESI†). A very small elongation of the N1–C1 and N1–C5 bond lengths (by 0.015 and 0.021 Å, respectively) can be observed on passing from **L** to $[HL]^+$ resulting from the protonation at the nitrogen atom, also accompanied by differences in the Se–C5 distances, while the rest of the molecule remains almost unchanged (Fig. S5, Table S7, ESI†). At the same time, the

natural charge on N1 becomes more positive, passing from −0.517 |e| in **L** to 0.254 |e| in $[\mathbf{HL}]^+$, while an opposite trend can be observed for Se1, whose charge amounts to 0.568 |e| in **L** and 0.172 |e| in $[\mathbf{HL}]^+$. The frontier Kohn–Sham molecular orbitals (KS-MOs) are delocalized and π in nature in both **L** and $[\mathbf{HL}]^+$, while the lone pairs (LPs) of electrons on N1 and Se1 in **L** correspond to MOs KS-HOMO−4 and KS-HOMO−6, respectively (Fig. S7, ESI†).

The I_2 molecule and $[I_2Cl]^-$ anion were also optimized in the gas phase. I_2 shows a calculated I–I bond length of 2.683 Å, corresponding to a Wiberg bond index (WBI) of 1.020. This distance, which is very close to that determined in the gas phase (2.67 Å),[35b,35c] and shorter than that observed for solid I_2 [2.715(6) Å],[35a] and for the co-crystallized I_2 molecule in **2** [I7–I7^i = 2.7420(11) Å, see Fig. 2], reflects the effect of intermolecular solid-state interactions in the latter systems. For the optimized $[I_2Cl]^-$ anion, the I–I and I–Cl distances are 2.945 and 2.640 Å (WBI = 0.580 and 0.464, respectively), indicating a three-body system nature for this anion in the gas phase, which can be described by a slightly unbalanced 3c–4e bonding scheme.[44] These calculated I–I and I–Cl bond lengths in the $[I_2C]^-$ anion differ from those observed in **2** for the $[I_2Cl]^-$ anion, being longer and shorter, respectively, than the corresponding experimental ones. The two Raman-active stretching modes for the $[I_2Cl]^-$ anion calculated in the gas phase fall at 133 and 221 cm^{-1}, the former featuring a major contribution from the ν(I–I) stretching vibration, and the latter from the ν(I–Cl) one.

Different model systems were also optimized (see Scheme 2), to consider the chemical environment of the structural synthons involved in the formation of **2**.

In particular, the geometry of the isolated adduct $\{[\mathbf{HL}]^+\cdots[Cl–I–I]^-\}$ (**I**) was optimized as a means of modelling the H-bond interaction between the $[\mathbf{HL}]^+$ cation and $[I_2Cl]^-$ anion (Tables S8, S9 and Fig. S8, ESI†). In the optimized structure, a further twisting of the ligand with respect to the free $[\mathbf{HL}]^+$ cation can be observed (τ = 29.5°). The N1–H1···Cl1 system diverges from linearity (N–H–Cl angle = 161°) more than the $[I_2Cl]^-$ moiety (I–I–Cl angle = 176°), and the H-bond interaction between the two ions is almost orthogonal (H1···Cl1–I1 angle = 85°, Fig. S5, ESI†). A lengthening of the N1–H1 bond distance of about 0.07 Å as compared to free $[\mathbf{HL}]^+$ cation results from the interaction with the $[I_2Cl]^-$ anion, accompanied by an increased negative natural charge on the nitrogen atom (−0.532 |e| see above). The interaction is calculated as a strong H-bond in the second order perturbation analysis (SOPTA) of the Fock matrix at the NBO level, the energy of the charge-transfer (CT) from the 3*p* LPs on the Cl atom to the N–H group amounting to about 100 kcal mol^{-1}. As a consequence, a weakening of the Cl–I interaction in the $\{[\mathbf{HL}]^+\cdots[Cl–I–I]^-\}$ (**I**) assembly (2.911 Å) with respect to free $[I_2Cl]^-$ (2.640 Å) was calculated, while the di-iodine moiety results very poorly perturbed and can be assimilated to a free I_2 unit, as shown by the calculated I–I bond distance in $\{[\mathbf{HL}]^+\cdots[Cl–I–I]^-\}$ (2.767 Å) and the calculated wavenumber of the Raman-active vibration having a major contribution from the ν(I–I) stretching (178 cm^{-1}). Summarily, the H-bonding interaction between the $[\mathbf{HL}]^+$ cation and the $[I_2Cl]^-$ anion results in the $[I_2Cl]^-$ anion behaving as a $I_2{\cdot}Cl^-$ system (weak CT adduct between I_2 and Cl^-). Accordingly, the I–Cl WBI is lowered to 0.211 as compared to 0.464 in free $[I_2Cl]^-$, and the Raman-active band with a major contribution from the ν(I–Cl) stretching, calculated at 143 cm^{-1} in the ionic pair assembly, assumes a negligible activity (0.8).

A comparison between structural and optimized data (Table S9, ESI†) indicates that the distance between the nitrogen and the chlorine atom optimized for **I** is shorter (by about 0.17 Å) than the distance observed in the crystal structure of **2**. Consequently, the optimized I–Cl distance is longer (by 0.19 Å) than the experimental one, while the I–I bond length is only slightly underestimated (by 0.05 Å). The computation on the isolated model system **I** thus results in a H-bond interaction stronger than the experimental one found in the crystal structure of **2**, whose nature is influenced by the rest of the non-covalent interactions present in the packing.

The geometry of the alternative $\{[\mathbf{HL}]^+\cdots[I–I–Cl]^-\}$ system (**II** in Scheme 2), formed through a N–H···I interaction, was also optimized (Fig. S8 and Tables S9, S10, ESI†) in order to account for the fact that its formation is not observed in the reaction between **L** and ICl. Both the N1–H1···I1 (162°) and I–I–Cl (176°) optimized angles are similar to those calculated for the corresponding angles in the model **I**, while the interaction between the two ions results in a smaller angle between the two synthons (H1–I1–I2 angle = 72°). The lengthening of the N1–H1 bond distance with respect to free $[\mathbf{HL}]^+$ amounts to 0.04 Å (as compared to $\Delta_{d(N–H)}$ = 0.07 Å between $[\mathbf{HL}]^+$ and **I**, see above), testifying for a weaker H-bond interaction in **II**. This is reflected in a smaller perturbation of I–Cl (2.501 Å) and I–I (3.074 Å) distances as compared to free $[I_2Cl]^-$ (see above). Accordingly, the energy of the H1···I1 interaction in $\{[\mathbf{HL}]^+\cdots[I–I–Cl]^-\}$ (**II**) calculated by SOPTA is only 54 kcal mol^{-1}.

To simulate the environment around the co-crystallized I_2 molecule (I7–I7^i) in **2**, the geometry of the *Z*-shaped $\{[Cl–I–I]^-\cdots I_2\cdots[I–I–Cl]^-\}$ assembly (**III**, Scheme 2) was successfully optimized in the gas phase (Tables S11, S12 and Fig. S9, ESI†). A stretched *Z*-shaped geometry is observed for the optimized system, with a calculated $ClI_2\cdots I$–I angle (about 130°) being

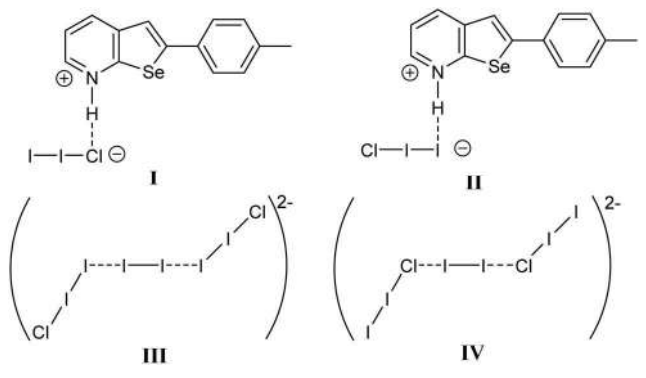

Scheme 2 Molecular models considered by means of DFT calculations.

much larger than the corresponding experimental one observed for the $[I_6Cl_2]^{2-}$ assembly in **2** (about 100°). Moreover, the calculated structural parameters for the $[I_2Cl]^-$ anions in the optimized fragment **III** (I–Cl = 2.637, I–I = 2.940 Å) are almost the same as those calculated for the isolated $[I_2Cl]^-$ in the gas phase and therefore under- (I–Cl) and over-estimated (I–I) distances, respectively, as compared to the corresponding structural values (see above). This indicates a very weak interaction between the trihalides and the bridging I_2 molecule, in agreement with the corresponding low interaction energy (6.8 kcal mol^{-1}) calculated by SOPTA. Despite this, the optimized model assembly **III** reproduces well the chemical environment experienced by the bridging I_2 molecule in the crystal structure of **2**, with the calculated I–I bond distance (2.743 Å, WBI = 0.797) differing by only 0.045 Å from structural data. The bridging I_2 molecule in the model system **III** (Scheme 2) assembly is, therefore, only slightly perturbed as compared to di-iodine in the solid state [2.715(6) Å],[35a] as typically found in systems featuring an I_2 molecule bridging two donor moieties.[25] The corresponding stretching mode was calculated at 168 cm^{-1} and features a very strong Raman activity.

The two model systems **II** and **III** optimized as structural synthons of **2**, show the $[I_2Cl]^-$ anion in two limit cases: an almost unperturbed trihalide [d_{I-Cl} = 2.64 Å, ν(I–Cl) = 220 cm^{-1}], and a strongly perturbed $I_2{\cdot}Cl^-$ system [d_{I-Cl} = 2.91 Å with an almost inactive Raman band at a calculated wavenumber as low as 140 cm^{-1} for the stretching mode with a major contribution from the ν(I–Cl) stretching]. In **2**, the observed I–Cl bond distances (2.695–2.702 Å) are in between those calculated for the two synthons **III** and **II**. On the basis of this analysis, the Raman spectrum recorded for **2** can be interpreted as follow: the peak at 171 cm^{-1} can be attributed to the ν(I–I) stretching of the co-crystallized I_2 molecule interacting with the $[I_2Cl]^-$ anions, the peak at 157 cm^{-1} can be assigned to the I_2 moiety of the trihalides, while the band at 76 cm^{-1} should correspond to the bending mode of the $[I_2Cl]^-$ anions, which is calculated at around 80 cm^{-1} with a weak Raman activity in all three systems $[I_2Cl]^-$, $\{[Cl–I–I]^-\cdots I_2\cdots[I–I–Cl]^-\}$ (**III**) and $\{[HL]^+\cdots[Cl–I–I]^-\}$ (**II**).

The alternative $\{[I–I–Cl]^-\cdots I_2\cdots[Cl–I–I]^-\}$ (**IV**, Scheme 2) assembly featuring $[I_2Cl]^-$ interacting with the central I_2 molecule through the Cl atom was also optimized (Tables S12, S13 and Fig. S9, ESI†). A further opening of the $I_2Cl\cdots I–I$ angle (144°) is observed. In this case the perturbation of the $[I_2Cl]^-$ anion resulting from the interaction with the I_2 molecule, is slightly larger (d_{I-I} = 2.932 Å, d_{I-Cl} = 2.645 Å), suggesting a marginally stronger interaction with the bridging I_2, also testified by the calculated longer I–I distance in the latter (2.753 Å). Nevertheless, the SOPTA-calculated energy for each $[I_2Cl]^-\cdots I_2$ interaction is 7.1 kcal mol^{-1}; therefore, the assembly **IV** is only 0.3 kcal mol^{-1} more stable than **III**.

Experimental

Materials, instrumentation and methods

All syntheses were carried out in air 2-(*p*-Tolyl)selenopheno [2,3-*b*]pyridine (**L**) was prepared according to procedures reported previously.[29] Reagents and solvents were used as purchased from Aldrich. Elemental analyses were performed with an EA1108 CHNS-O Fisons instrument (T = 1000 °C). Raman spectroscopy experiments were performed using aRenishaw inVia conventional Raman microscope (in back-scattered geometry), in conjunction with a Leica DM2500 M optical microscope. Its fibre-coupled laser module (NIR Diode) emits at 785 nm, in a line focus of approx. 25 μm. Raman signals were recorded by a fibre-coupled grating spectrometer [1200 l mm^{-1} (633/780)], with a (Peltier cooled) Renishaw CCD camera (using a spectral step size of 1.3 cm^{-1}, at 500 cm^{-1}). The laser power was kept at 0.05% of maximum (~2.2 mW) to avoid sample melting; no sample decomposition was observed during experiments. The values in parentheses next to the ν(I–I) values represent the intensities of the peaks relative to the strongest, taken equal to 100 (peaks with relative intensities lower than 1 are not reported).

Synthesis of 1 and 2

To a vial containing a 2.75×10^{-3} M solution of **L** in acetonitrile (2.0 mL, 5.5×10^{-6} mol) an equimolar amount of ICl in the same solvent was added (C = 0.25 M, V = 22 μL). After several weeks at room temperature in the air, the slow evaporation of part of the solvent resulted in the formation of a small amount of crystals of two different morphologies difficult to separate: lath shaped colorless crystals and dark-red blocks, corresponding to **1** and **2**, respectively. The remaining solvent was pipetted away and the crystals, washed with diethyl ether, were picked up manually for X-ray characterization. Crystals of both facies resulted very stable in the air at room temperature for a long time. The serendipity of the crystallization process and the hand collection of the crystals prevented the evaluation of reaction yields. **1**: elemental analysis (%) calcd for $C_{14}H_{16}ClNO_2Se$ (344.69): C 48.78, H 4.68, N 4.06; found: C 48.74, H 4.58, N 4.00. **2**: elemental analysis (%) calcd for $C_{14}H_{12}ClI_{2.33}NSe$ (604.76): C 27.81, H 1.99, N 2.32; found: C 27.75, H 1.95, N 2.28. Mp: 71 °C (decomposition). Raman in the range 500–65 cm^{-1} ν(I–I) (relative intensity): 171 (5.4), 157 (10), 76 (3.0).

X-Ray crystallography

Single Crystal X-ray Diffraction data for compound **1** were collected at 100 K on a Rigaku 007HF diffractometer, equipped with Varimax confocal mirrors, an AFC11 goniometer, a HyPix 6000 detector and an Oxford Cryosystems low temperature device. Data for compound **2** were collected at 100 K on a Rigaku FRE+ diffractometer, equipped with HF Varimax confocal mirrors, an AFC12 goniometer, an HG Saturn 724+ CCD area detector and an Oxford Cryosystems low temperature device. Data collection and reduction were carried out using CrysAlisPro[45] 1.171.40.37a as the graphical interface. Both crystal structures were solved with ShelXT[46] 2018/2 solution program using a dual-space algorithm and by using Olex2[47] 1.5 as the graphical interface. The models were refined with ShelXL[45] 2018/3 using full matrix least squares minimisation on F^2. For compound **1**, a H atom for each water molecule was

refined over two sites with equal atomic occupancies. For compound **2**, the disordered I2, I4, and I6 atoms were refined over two positions with occupancies: I2A\I2B 92 : 8, I4A\I4B 56 : 44, I6A\I6B 43 : 57 making use of thermal and geometrical restrains. CCDC: 2204970, 2204971.†

DFT calculations

The computational investigation was carried out at the DFT level[39] with the Gaussian 16[48] suite of programs and employing Adamo and Barone's mPW1PEW hybrid functional[40] along with the LANL2DZ(d,p) basis set (featuring both diffuse and polarization functions)[41] with effective core potentials (ECP).[42,43] Basis sets were extracted from the EMSL BS Library.[49] The molecular geometry optimizations were performed starting from structural data, when available. Fine numerical integration grids (Integral = ultrafine keyword) were used, and the nature of minimum of each optimized structure was verified by harmonic frequency calculations (freq = Raman keyword). PES scans were performed by imposing the rotation of the *p*-tolyl ring (between 0 and 180°, steps of 10°) and optimizing the resulting geometry at each rotational step (opt = modredundant keyword). A natural population analysis was carried out at the optimized geometries using the natural bonding orbital (NBO) partitioning scheme.[50] Investigation of the optimized structures and the shapes of KS-MOs employed the programs GaussView 6.0.16[51] and Chemissian 4.53.[52]

Conclusions

Although the chemistry of polyhalides $[X_n(X_2)_m]^{n-}$ or $[X_{2m+n}]^{n-}$ (n, $m > 0$; X = halogen) has greatly expanded over the past decades and their nature has been examined in depth, much work still has to be done to explore the fascinating class of polyinterhalides of the type $[X_n(Y_2)_m]^{n-}$ or $[X_n(YZ)_m]^{n-}$ (X, Y, Z = halogen), which in principle would be characterized by an increased structural diversity with respect to homonuclear variants. In this paper we have described a rare example of polyinterhalogen anion made of $[I_2Cl]^-$ and I_2. The resulting discrete *H*-shaped $[I_{10}Cl_4]^{4-}$ polyanion is the result of a delicate interplay in the solid state between directional intermolecular hydrogen bonds (HBs), halogen-bonds (XBs) and π–π interactions driven by the structural features of the 2-(*p*-tolyl) selenopheno[2,3-*b*]pyridinium cation template, as demonstrated by DFT calculations. This study also points out the great tendency of donor molecules featuring the simultaneous presence of both N-heterocyclic and chalcogen atoms to react at the nitrogen sites with di-halogens and interhalogens leaving the chalcogen Lewis donor sites not involved.

Author contributions

Conceptualisation: VL, AP, MA, EP. Data curation: MA, AP, EP, SJC, JBO, VL. Investigation: AP, EP, SJC, JBO, GP, RFS, RHB. Supervision: VL, AP. Writing (original draft): VL, AP. Writing (reviewing ad editing): all authors. Funding acquisition: VL, GP, EJL. Validation: all authors.

Conflicts of interest

There are no conflicts to declare.

Acknowledgements

Mr Nikolay Zhelev (University of Southampton) is kindly acknowledged for the Raman spectroscopy measurements reported in the present study and to Prof. Andrea Russell (University of Southampton) for access to the Raman microscope. This study was financed in part by the Coordenação de Aper-feiçoamento de Pessoal de Nível Superior - Brasil (CAPES) - Finance Code 001. FAPERGS (PqG 21/2551-0002094-6 and PqG 19/2551-0001867-3), CNPq (Universal 422645/2021-4), FINEP and the University of Cagliari are acknowledged for financial support.

Notes and references

1 L. C. Gilday, S. W. Robinson, T. A. Barendt, M. J. Langton, B. R. Mullaney and P. D. Beer, *Chem. Rev.*, 2015, **115**, 7118–7195.
2 S. Tothadi and G. R. Desiraju, *Chem. Commun.*, 2013, **49**, 7791–7793.
3 S. Tothadi, P. Sanphui and G. R. Desiraju, *Cryst. Growth Des.*, 2014, **14**, 5293–5302.
4 A. Mukherjee, S. Tothadi and G. R. Desiraju, *Acc. Chem. Res.*, 2014, **47**, 2514–2524.
5 C. B. Aakeroy, M. Fasulo, N. Schultheiss, J. Desper and C. Moore, *J. Am. Chem. Soc.*, 2007, **129**, 13772–13773.
6 H. Jain, D. Sutradhar, S. Roy and G. R. Desiraju, *Angew. Chem., Int. Ed.*, 2021, **60**, 12841–12846.
7 C. C. Robertson, J. S. Wright, E. J. Carrington, R. N. Perutz, C. A. Hunter and L. Brammer, *Chem. Sci.*, 2017, **8**, 5392–5398.
8 P. M. J. Szell, G. Cavallo, G. Terraneo, P. Metrangolo, B. Gabidullin and D. L. Bryce, *Chem. – Eur. J.*, 2018, **24**, 11364–11376.
9 S. Scheiner, *Molecules*, 2021, **26**, 350.
10 (*a*) A. J. Blake, F. A. Devillanova, R. O. Gould, W.-S. Li, V. Lippolis, S. Parsons, C. Radek and M. Schröder, *Chem. Soc. Rev.*, 1998, **27**, 195–206; (*b*) P. H. Svensson and L. Kloo, *Chem. Rev.*, 2003, **103**, 1649–1684; (*c*) M. Arca, F. Demartin, F. A. Devillanova, A. Garau, F. Isaia, V. Lippolis and G. Verani, *J. Chem. Soc., Dalton Trans.*, 1999, 3069–3073; (*d*) M. Savastano, *Dalton Trans.*, 2021, **50**, 7022–7025.
11 (*a*) C. J. Horn, A. J. Blake, N. R. Champness, V. Lippolis and M. Schröder, *Chem. Commun.*, 2003, 1488–1489; (*b*) C. J. Horn, A. J. Blake, N. R. Champness, V. Lippolis and M. Schröder, *Chem. Commun.*, 2003, 312–313;

(*c*) M. Savastano, C. Bazzicalupi and A. Bianchi, *Dalton Trans.*, 2022, **51**, 10728–10739.

12 (*a*) H. Paulsson, M. Berggrund, E. Svantesson, A. Hagfeldt and L. Kloo, *Sol. Energy Mater. Sol. Cells*, 2004, **82**, 345–360; (*b*) A. A. Petrov and A. B. Tarasov, *Front. Chem.*, 2020, **8**, 418; (*c*) K. Kakiage, T. Tokutome, S. Iwamoto, T. Kyomen and M. Hanaya, *Chem. Commun.*, 2012, **49**, 179–180.

13 (*a*) H. Wang, H. Li, B. Xue, Z. Wang, Q. Meng and L. Chen, *J. Am. Chem. Soc.*, 2005, **127**, 6394–6401; (*b*) E. Pulli, E. Rozzi and F. Bella, *Energy Convers. Manage.*, 2020, **219**, 112982.

14 (*a*) T. M. Beck, H. Haller, J. Streuff and S. Riedel, *Synthesis*, 2014, 740–747; (*b*) T. Schlama, K. Gabriel, V. Gouverneur and C. Mioskowski, *Angew. Chem., Int. Ed. Engl.*, 1997, **36**, 2342–2344.

15 (*a*) K. Sonnenberg, L. Mann, F. A. Redeker, B. Schmidt and S. Riedel, *Angew. Chem., Int. Ed.*, 2020, **59**, 5464–5493; (*b*) B. Schmidt, B. Schröder, K. Sonnenberg, S. Steinhauer and S. Riedel, *Angew. Chem., Int. Ed.*, 2019, **58**, 10340–10344; (*c*) H. Haller and S. Riedel, *Z. Anorg. Allg. Chem.*, 2014, **640**, 1281–1291; (*d*) C. Walbaum, M. Richter, U. Sachs, I. Pantenburg, S. Riedel, A.-V. Mudring and G. Meyer, *Angew. Chem., Int. Ed.*, 2013, **52**, 12732–12735; (*e*) A. Moghimi, R. Alizadeh, H. Aghabozorg, A. Shockravi, M. C. Aragoni, F. Demartin, F. Isaia, V. Lippolis, A. Harrison, A. Shokrollahi and M. Shamsipur, *J. of Mol. Struct.*, 2005, **705**, 166–173.

16 Z. Yin, Q.-X. Wang and M.-H. Zeng, *J. Am. Chem. Soc.*, 2012, **134**, 4857–4863.

17 (*a*) Z. Fei, F. D. Bobbink, E. Păunescu, R. Scopelliti and P. J. Dyson, *Inorg. Chem.*, 2015, **54**, 10504–10512; (*b*) V. K. Thorsmølle, J. C. Brauer, S. M. Zakeeruddin, M. Grätzel and J.-E. Moser, *J. Phys. Chem. C*, 2012, **116**, 7989–7992.

18 (*a*) M. C. Aragoni, M. Arca, F. A. Devillanova, M. B. Hursthouse, S. L. Huth, F. Isaia, V. Lippolis and A. Mancini, *CrystEngComm*, 2004, **6**, 540–542; (*b*) M. C. Aragoni, M. Arca, F. A. Devillanova, F. Isaia, V. Lippolis, A. Mancini, L. Pala, A. M. Z. Slawin and J. D. Woollins, *Chem. Commun.*, 2003, 2226–2227.

19 (*a*) G. Ciancaleoni, M. Arca, G. F. Caramori, G. Frenking, F. S. S. Schneider and V. Lippolis, *Eur. J. Inorg. Chem.*, 2016, 3804–3812; (*b*) M. C. Aragoni, M. Arca, F. A. Devillanova, F. Isaia and V. Lippolis, *Cryst. Growth Des.*, 2012, **12**, 2769–2779.

20 (*a*) M. C. Aragoni, M. Arca, C. Caltagirone, C. Castellano, F. Demartin, A. garau, F. Isaia, V. Lippolis, R. Montis and A. Pintus, *CrystEngComm*, 2012, **14**, 5809–5823; (*b*) M. C. Aragoni, M. Arca, F. A. Devillanova, M. B. Hursthouse, S. L. Huth, F. Isaia, V. Lippolis, A. Mancini and G. Verani, *Eur. J. Inorg. Chem.*, 2008, 3921–3928; (*c*) M. C. Aragoni, M. Arca, F. A. Devillanova, M. B. Hursthouse, S. L. Huth, F. Isaia, V. Lippolis, A. Mancini and H. Olgive, *Inorg. Chem. Commun.*, 2005, **8**, 79–82.

21 (*a*) M. C. Aragoni, M. Arca, S. J. Cole, F. A. Devillanova, M. B. Hursthouse, S. L. Coles (nèè Huth), F. Isaia, V. Lippolis and A. Mancini, *CrystEngComm*, 2011, **13**, 6319–6322; (*b*) R. B. Bailey, G. W. Drake, M. Grabarczyk, T. W. Hanks, L. L. Hook and W. T. Pennington, *J. Chem. Soc., Perkin Trans.*, 1997, **2**, 2773–2779; (*c*) T. Uchida and K. Kimura, *Acta Crystallogr., Sect. C: Cryst. Struct. Commun.*, 1984, **40**, 139–140; (*d*) R. Bailey Walsh, C. W. Padgett, P. Metrangolo, G. Resnati, T. W. Hanks and W. T. Pennington, *Cryst Growth Des.*, 2001, **1**, 165–175.

22 (*a*) E. L. Rimmer, R. D. Bailey, T. W. Hanks and W. T. Pennington, *Chem. – Eur. J.*, 2000, **22**, 4071–4081; (*b*) R. H. Jones, K. S. Knight, W. G. Marshall, J. Clews, R. J. Darton, D. Pyatt, S. J. Coles and P. N. Horton, *CrystEngComm*, 2014, **16**, 237–243; (*c*) M. C. Aragoni, M. Arca, F. A. Devillanova, M. B. Hursthouse, S. L. Huth, F. Isaia, V. Lippolis, A. Mancini, H. R. Ogilvie and G. Verani, *J. Organomet. Chem.*, 2005, **690**, 1923–1934; (*d*) F. F. Awwadi, D. Taher, M. H. Kailani, M. I. Alwahsh, F. Odeh, T. Ruffer, D. Schaarschmidt and H. Lang, *Cryst. Growth Des.*, 2020, **20**, 543–551.

23 S. Aroson, P. Epstein, B. D. Aroson and G. Wieder, *J. Phys. Chem.*, 1982, **86**, 1035–1037.

24 (*a*) V. Nemec, K. Lisac, V. Stilinović and D. Cinčić, *J. Mol. Struct.*, 2017, **1128**, 400–409; (*b*) A. S. Batsanov, J. A. K. Howard, A. P. Lightfoot, S. J. R. Twiddle and A. Whiting, *Eur. J. Org. Chem.*, 2005, 1876–1883; (*c*) O. Hassel and H. Hope, *Acta Chem. Scand.*, 1961, **15**, 407–416; (*d*) E. Kukkonen, H. Malinen, M. Haukka and J. Knonu, *Cryst. Growth Des.*, 2019, **19**, 2434–2445.

25 F. Isaia, M. C. Aragoni, M. Arca, F. Demartin, F. A. Devillanova, G. Ennas, A. Garau, V. Lippolis, A. Mancini and G. Verani, *Eur. J. Inorg. Chem.*, 2009, 3667–3672.

26 (*a*) M. Arca, F. Demartin, F. A. Devillanova, A. Garau, F. Isaia, V. Lippolis and G. Verani, *Trends Inorg. Chem.*, 1999, **6**, 1–18; (*b*) P. D. Boyle and S. M. Godfrey, *Coord. Chem. Rev.*, 2001, **223**, 265–299; (*c*) A. Garau, F. Isaia, V. Lippolis, A. Mancini and G. Verani, *Bioinorg. Chem. Appl.*, 2006, **1**, 1–12.

27 E. L. Rimmer, R. D. Bailey, W. T. Pennington and T. W. Hanks, *J. Chem. Soc., Perkin Trans.*, 1998, **2**, 2557–2562.

28 R. Montis, M. Arca, M. C. Aragoni, A. J. Blake, C. Castellano, F. Demartin, F. Isaia, V. Lippolis, A. Pintus, E. J. Lenardão, G. Perin, A. E. O'Connor and S. Thurow, *New J. Chem.*, 2018, **42**, 10592–10602.

29 (*a*) T. J. Peglow, R. H. Bartz, C. C. Martins, A. L. Belladona, C. Luchese, E. A. Wilhelm, R. F. Schumacher and G. Perin, *ChemMedChem*, 2020, **15**, 1741–1751; (*b*) G. Perin, T. J. Peglow, R. H. Bartz, R. Cargnelutti, E. J. Lenardão and R. F. Schumacher, *Arkivoc*, 2019, **part ii**, 50–64.

30 M. C. Aragoni, M. Arca, F. A. Devillanova, A. Garau, F. Isaia, V. Lippolis and G. Verani, *Dalton Trans.*, 2005, 2252–2258.

31 (*a*) N. Bricklebank, S. M. Godfrey, C. A. McAuliffe and R. G. Prichard, *J. Chem. Soc., Dalton Trans.*, 1993, 2261–2266; (*b*) N. N. Greenwood and A. Earnshaw, *Chemistry of the Elements*, Pergamon, New York, 1984; (*c*) E. J. Juárez-Pérez, M. C. Aragoni, M. Arca, A. J. Blake,

F. A. Devillanova, A. Garau, F. Isaia, V. Lippolis, R. Núñez, A. Pintus and C. Wilson, *Chem. Eur. J.*, 2011, **17**, 11497–11514.
32 A. Bondi, *J. Phys. Chem.*, 1964, **68**, 441–451.
33 Y. Q. Wang, Z. M. Wang, C. S. Liao and C. H. Yan, *Acta Crystallogr., Sect. C: Cryst. Struct. Commun.*, 1999, **55**, 1503–1506.
34 T. Horibe, Y. Tsuji and K. Ishihara, *ACS Catal.*, 2018, **8**, 6362–6366.
35 (*a*) F. van Bolhuis, P. B. Koster and T. Migchelsen, *Acta Crystallogr.*, 1967, **23**, 90–91; (*b*) C. Van Der Marel, W. Bras and W. Van Der Lugt, *Mol. Phys.*, 1988, **64**, 445–456; (*c*) I. L. Karle, *J. Chem. Phys.*, 1955, **23**, 1739.
36 (*a*) G. V. Shilov, O. N. Kazheva, O. A. D'yachenko, M. S. Chernov'yants, S. S. Simonyan, V. E. Gol'eva and A. I. Pyshchev, *Zh. Fiz. Khim. (Russ.) (Russ. J. Phys. Chem)*, 2002, **76**, 1436–1443; (*b*) M. T. Johnson, Z. Džolić, M. Cetina, O. F. Wendt, L. Öhrstrom and K. Rissanen, *Cryst. Growth Des.*, 2012, **12**, 362–368; (*c*) L. Meazza, J. Martì-Rujas, G. Terraneo, C. Castiglioni, A. Milani, T. Pilati, P. Metrangolo and G. Resnati, *CrystEngComm*, 2011, **13**, 4427–4435.
37 A. J. Blake, R. O. Gould, W.-S. Li, V. Lippolis, S. Parsons, C. Radek and M. Schröder, *Inorg. Chem.*, 1998, **37**, 5070–5077.
38 M. Wolff, A. Okrut and C. Feldmann, *Inorg. Chem.*, 2011, **50**, 11683–11694.
39 W. Koch and M. C. Holthausen, *A chemist's guide to density functional theory*, Wiley-VCH, New York, 2001.
40 C. Adamo and V. Barone, *J. Chem. Phys.*, 1998, **108**, 664–675.
41 C. E. Check, T. O. Faust, J. M. Bailey, B. J. Wright, T. M. Gilbert and L. S. Sunderlin, *J. Phys. Chem. A*, 2001, **105**, 8111–8116.
42 T. H. Dunning and P. J. Hay, in *Methods of Electronic Structure Theory*, ed. H. F. Schaefer, Plenum Press, New York, 1977, vol. 2, p. 1.
43 J. V. Ortiz, P. J. Hay and R. L. Martin, *J. Am. Chem. Soc.*, 1992, **114**, 2736–2737.
44 W. Holzer, W. F. Murphy and H. J. Bernstein, *J. Chem. Phys.*, 1970, **52**, 399–407.
45 CrysAlisPro Software System, Rigaku Oxford Diffraction, 2020.
46 G. M. Sheldrick, *Acta Crystallogr., Sect. A: Found. Adv.*, 2015, **71**, 3–8.
47 O. V. Dolomanov, L. J. Bourhis, R. J. Gildea, J. A. K. Howard and H. Puschmann, *J. Appl. Crystallogr.*, 2009, **42**, 339–341.
48 M. J. Frisch, G. W. Trucks, H. B. Schlegel, G. E. Scuseria, M. A. Robb, J. R. Cheeseman, G. Scalmani, V. Barone, G. A. Petersson, H. Nakatsuji, X. Li, M. Caricato, A. V. Marenich, J. Bloino, B. G. Janesko, R. Gomperts, B. Mennucci, H. P. Hratchian, J. V. Ortiz, A. F. Izmaylov, J. L. Sonnenberg, D. Williams-Young, F. Ding, F. Lipparini, F. Egidi, J. Goings, B. Peng, A. Petrone, T. Henderson, D. Ranasinghe, V. G. Zakrzewski, J. Gao, N. Rega, G. Zheng, W. Liang, M. Hada, M. Ehara, K. Toyota, R. Fukuda, J. Hasegawa, M. Ishida, T. Nakajima, Y. Honda, O. Kitao, H. Nakai, T. Vreven, K. Throssell, J. A. Montgomery, J. E. Peralta, F. Ogliaro, M. J. Bearpark, J. J. Heyd, E. N. Brothers, K. N. Kudin, V. N. Staroverov, T. A. Keith, R. Kobayashi, J. Normand, K. Raghavachari, A. P. Rendell, J. C. Burant, S. S. Iyengar, J. Tomasi, M. Cossi, J. M. Millam, M. Klene, C. Adamo, R. Cammi, J. W. Ochterski, R. L. Martin, K. Morokuma, O. Farkas, J. B. Foresman and D. J. Fox, Gaussian 16, Wallingford, CT, 2016.
49 B. P. Pritchard, D. Altarawy, B. Didier, T. D. Gibson and T. L. Windus, *J. Chem. Inf. Model.*, 2019, **59**, 4814–4820.
50 A. E. Reed, R. B. Weinstock and F. Weinhold, *J. Chem. Phys.*, 1985, **83**, 735–746.
51 R. D. Dennington, T. A. Keith and J. M. Millam, GaussView 6.0. 16, Semichem Inc., Shawnee Mission KS, 2016.
52 L. V. Skripnikov, Chemissian Version 4.53, Visualization Computer Program, 2017.